Sensors and Actuators A 201 (2013) 254–263

Contents lists available at ScienceDirect

Sensors and Actuators A: Physical

journal homepage: www.elsevier.com/locate/sna

A novel background interferences elimination method in electronic nose using pattern recognition

Lei Zhang[a,*], Fengchun Tian[a], Lijun Dang[a], Guorui Li[a], Xiongwei Peng[a], Xin Yin[a], Shouqiong Liu[b]

[a] College of Communication Engineering, Chongqing University, 174 ShaZheng Street, ShaPingBa District, Chongqing 400044, China
[b] Academy of Metrology and Quality Inspection, Chongqing 401123, China

ARTICLE INFO

Article history:
Received 23 March 2013
Received in revised form 21 May 2013
Accepted 25 July 2013
Available online 2 August 2013

Keywords:
Electronic nose
Sensor array
Odor interference
Counteraction
Pattern recognition

ABSTRACT

Metal oxide semiconductor (MOS) sensor array with some cross-sensitivities to target gases is often used in electronic nose (E-nose) combined with signal processing techniques for indoor air contaminants monitoring. However, MOS sensors have some intrinsic flaw of high susceptibility to background interference which would seriously destroy the specificity and stability of electronic nose in practical application. This paper presents an on-line counteraction of unwanted odor interference based on pattern recognition for the first time. Six kinds of target gases and four kinds of unwanted odor interferences were experimentally studied. First, two artificial intelligence learners including a multi-class least square support vector machine (learner-1) and a binary classification artificial neural network (learner-2) are developed for discrimination of unwanted odor interferences. Second, a real-time dynamically updated signal matrix is constructed for correction. Finally, an effective signal correction method was employed for E-nose data. Experimental results in the real cases studies demonstrate the effectiveness of the presented model in E-nose based on MOS gas sensors array.

1. Introduction

Electronic nose (E-nose), which employs an array of chemical gas sensors, has been widely used for environmental pollution monitoring. An E-nose is an instrument consisting of an array of reversible but only semi-selective gas sensors coupled with a series of pattern recognition algorithms. Chemical sensors as transducers that incorporate a chemical detection layer and transform a chemical interaction into a measurable electrical signal have often been used for environmental monitoring. The ideal gas sensor would exhibit reliability, robustness, sensitivity, selectivity and reversibility [1]. Gas sensors, based on the chemical sensitivity of metal oxide semi-conductors (MOS), are readily available commercially. They have been more widely used to make arrays for odor measurement than any other class of gas sensors. Resistance changes due to combustion reactions occurring within the lattice oxygen species on the surface of metal oxide particles [2,3]. MOS sensors respond to a broad range of analytes such as formaldehyde, benzene, toluene, ketone, carbon monoxide, carbon dioxide, nitrogen dioxide and ammonia.

However, MOS sensors have also some intrinsic flaws which can be concluded as four kinds of background interferences in electronic nose. First, they are susceptive to environmental parameters such as temperature which has been called direct interferences [4] for the electronic nose data in practical applications. Second, drift is defined as the temporal shift of sensor response under constant physical and chemical conditions. The reasons for drift are unknown dynamic processes in the sensor system, e.g. poisoning or aging of sensors, or environmental parameters change [5]. In addition, MOS sensors have instrument related signal shift and baseline differences in measurement data. That is, the sensor of completely identical type has different response to analytes with the same condition (concentration, temperature and humidity). A fundamental assumption is that the inherent variability during sensor manufacturing process leads to the slight differences and signal shift in the reactivity of the tin oxide substrate of individual sensor [6]. Finally, MOS gas sensors have high susceptibility to unwanted odor interferences in human surroundings (e.g. perfume, ethanol, fruit smell and toiletwater). The kind of background odor interferences will directly trouble the metal oxide semiconductor sensors in the electronic nose system with high strength in practical environmental detection. The most serious problem is the false discrimination and concentration estimation of the measured target gases when the unwanted odors exist.

For solutions of the first three kinds of interferences (environmental fluctuation, sensor drift caused by aging and signal shift caused by sensor replacement), fortunately, many researchers have proposed different methods. Counteraction methods for

* Corresponding author. Tel.: +86 13629788369; fax: +86 23 65103544.
E-mail address: leizhang@cqu.edu.cn (L. Zhang).

0924-4247/$ – see front matter © 2013 Elsevier B.V. All rights reserved.
http://dx.doi.org/10.1016/j.sna.2013.07.032

background interferences caused by environmental fluctuation (the 1st interference) have been presented in [4,7–9]. Different compensation models of long-term sensor drift (the 2nd interference) have been fully investigated and tried in [5,10–14]. For the signal shift (the 3rd interference) between two identical sensors, calibration transfer models [15–17] have been successfully used for sensor standardization in an electronic nose. However, there is no research demonstrating the possible on-line counteraction of unwanted odor interference (the 4th interference) in an E-nose. That is, an E-nose will lose effectiveness when exposed to surroundings with unwanted background odor (e.g. perfume). Therefore, it is meaningful to present a on-line counteraction model of the 4th interference and eliminate the sensor "fault" of an E-nose caused by odor interferences in real time ambient air monitoring. The novelty of this paper is that we proposes an on-line counteraction model of background odor interferences based on artificial intelligence learners for real-time environmental monitoring for the first time and preliminarily resolves the problem of odor interferences. In addition, the background odor interferences are various in the real world, therefore, we seemed all unwanted odor interferences as one class in artificial intelligence learners and solved the variety problem of unwanted odor. The robust on-line counteraction model can be approximately divided into two parts: "fault" recognition and "fault" counteraction.

A number of pattern recognition algorithms have been widely used in E-nose such as artificial neural network (ANN) based methods [18,19], heuristic and bio-inspired methods [20,21], linear multivariate techniques and discrimination analysis [22,23] and support vector machine (SVM) based methods [24,25]. Literature comparisons demonstrate that SVM and ANN are better choices in classification than any other methods due to their higher accuracy and stronger robustness [26,27]. Besides, the previous research [25] also demonstrates the strong nonlinearity of electronic nose data. Thus, SVM and ANN were selected as the pattern recognition methods for fault recognition. Therefore, two learners (learner-1 and learner-2) were studied with subsequent counteraction, respectively. Learner-1 is based on multi-class mechanism and learner-2 is based on binary classification rule. For clarity, each gas is seemed as an independent class and multiple classes including an unwanted odor interferences class were constructed in learner-1. Consider that the key study of this paper is counteraction of odor interferences, we induce the multiple target gases classes into one class, and the odor interferences were induced as the second class in learner-2.

In the previous work, we introduced a heuristic and bio-inspired model for gases concentration estimation [21] and also proposed a multi-class classification model [25] in environmental monitoring. However, the background interference caused by unwanted odors result in failure of the estimation and classification models presented above. Therefore, in the present study, we develop a deep research on the on-line counteraction model of E-nose designed with metal oxide semiconductor sensors when exposed to strong odor interferences using two artificial intelligence learners (learner-1 and learner-2), respectively.

2. Materials and methods

2.1. Electronic nose system

The electronic nose system and experimental set up developed in this paper were described previously in [21]. Four metal oxide semiconductor gas sensors from FIGARO were used. They are TGS2602, TGS2620 and TGS2201 with two outputs A and B (TGS2201A/B). The sensing material in TGS gas sensors is metal oxide, most typically SnO_2. The detection principle of TGS sensors is based on chemical adsorption and desorption of gases on the sensor's surface. When a metal oxide crystal such as SnO_2 is heated at a certain high temperature in air, oxygen is adsorbed on the crystal surface with a negative charge and the crystal surface is formed to serve as a potential barrier against electron flow. The electrical resistance Rs of the sensor is attributed to this potential barrier. In the presence of a deoxidizing gas, the surface density of the negatively charged oxygen decreases, so that the electrical resistance Rs of sensor will decrease. Actually, the Rs varies from sensor to sensor, therefore, typical sensitivity characteristics are expressed as a ratio of Rs in various concentrations of gases over Ro in a certain concentration of a target gas. The species monitored by sensor array include *carbon monoxide*, *nitric oxide*, *nitrogen dioxide*, *ammonia*, *toluene*, *hydrogen*, *methane*, *hydride* and *VOCs*. A module with two auxiliary sensors for temperature and humidity compensations was also used as the inputs of prediction model. The sensors were mounted on a custom designed printed circuit board (PCB), along with associated electrical components. A 12-bit analog-digital converter (A/D) is used as interface between the FPGA (Field Programmable Gate Array) processor and the sensors. The system can be connected to the PC via a JTAG (Joint Test Action Group) port. In this paper, six kinds of target gases being monitored by the chemical electronic nose made in our laboratory include formaldehyde, benzene, toluene, carbon monoxide (CO), ammonia (NH_3) and nitrogen dioxide (NO_2). The experimental platform and the environmental electronic nose instrument made in our laboratory with its internal printed circuit board (PCB) have been described in Fig. 1. The corresponding circuit modules (e.g. sensor array, power module, CPU, SDRAM, and LCD) in PCB have also been designated. Note that the air sampler was used for sampling the gas in chamber and determining the concentration of the analyte using spectrophotometer and gas chromatography (GC) analysis. In preparations of each gas, formaldehyde, benzene and toluene are volatilized in a gas collecting bag with injection of their liquor and pure nitrogen (N_2) for dilution, respectively; while CO, NH_3 and NO_2 are diffused in a gas collecting bag with injection of their standard gas and pure nitrogen (N_2) for dilution, respectively. In experiments, the target gas is injected into the chamber with different time length through a flow-controlled pump connected with the gas collecting bag. The experimental target temperature was set as 15, 20, 25, 30 and 35 °C; the relative humidity was set as 40%, 60% and 80%RH. The total measurement cycle time for each experiment was set to 20 min, i.e., 2 min for baseline, 8 min for steady state response and 10 min for gas bleed. Each sample contains 350 sampling points.

2.2. Sensor signal preprocessing

Signal preprocessing in this work is used for smooth filtering and normalization of the continuous sampling points. Set the length of the smooth filter as n, the length of the observation signal vector S is N, and the filtered and normalized signal vector X can be obtained by

$$X(i) = \frac{\sum_{l=i}^{i+n-1} S(l) - \max\left\{S(i), \ldots, S(i+n-1)\right\} - \min\left\{S(i), \ldots, S(i+n-1)\right\}}{n-2}, \quad i = 1, \ldots, N-n+1 \tag{1}$$

$$X = \frac{X}{4095} \tag{2}$$

The normalization of formula (2) is that sensor responses were simply divided by 4095. It is worthy noting that the digit of 4095 (that

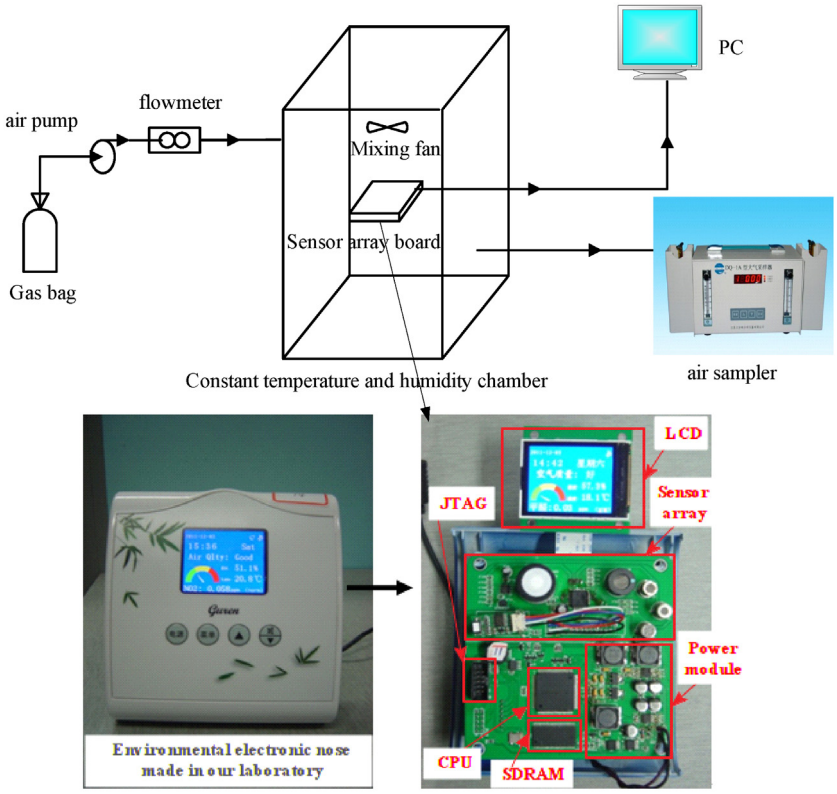

Fig. 1. Experimental platform (above) and the environmental electronic nose made in our laboratory with internal printed circuit board (PCB) (below).

is, $2^{12} - 1$) is the maximum value of the 12-bit A/D output for each sensor.

2.3. E-nose data preparation

This section will introduce five datasets, wherein dataset 1 is used for classification model learning and testing; dataset 2 and dataset 3 are used to reflect a real-world case study and validate the background elimination model in our E-nose.

2.3.1. Dataset 1 for classification model training

This paper aims to build a multi-classifier with seven objects: formaldehyde, benzene, toluene, carbon monoxide, ammonia, nitrogen dioxide and odor interferences. Four kinds of familiar odor interferences (e.g. perfume, ethanol, fruit smell (orange) and toiletwater) were tested. Note that the toiletwater that can be used to drive mosquito is composed of fragrance and alcohol. In classification model, the whole dataset was divided into train data and test data. The train samples were selected from the whole dataset by using KS algorithm [17] and the remaining samples were used as test data which has no relation with classification model establishment and only taken as performance validation of the classifier. The number of train samples for formaldehyde, benzene, toluene, CO, NH_3, NO_2, unwanted odor interference (ethanol and orange) are 125, 48, 44, 38, 40, 25, 40 (26 and 14); and the number of test samples are 63, 24, 22, 20, 20, 12, 19 (13 and 6). The concentrations of target gases for each sample are different. For formaldehyde, the concentration range is 0–10 ppm; for benzene, toluene, NH_3 and NO_2, the concentration range is 0–5 ppm; for CO, the concentration range is 1–60 ppm. The specific concentrations of the six contaminants for each experimental sample in different combinations of temperature and humidity (i.e. (15, 60) represents the experimental temperature 15 °C and relative humidity 60%RH) are described in Table 1 which has also been presented in our previous work [25]. It is worthy noting that the reason why we only use ethanol and orange for classifier design is to verify the robustness of the proposed on-line counteraction model when exposed to perfume and toiletwater in real time application.

2.3.2. Dataset 2 of real-time interference elimination without target gas

The dataset 2 was obtained when the electronic nose was exposed to the environment only with unwanted odor interferences, that is, no target gases were presented. An observation vector with length of 2480 points for each sensor was obtained in continuous sampling way. This dataset is developed under two odor interferences, respectively. In detail, we present the approximation positions for each object as follows. Perfume exists in two approximated regions 95–308 and 709–958; toiletwater exists in two approximated regions 1429–1765 and 2056–2265; the approximated interference regions have been illustrated by four Rectangular windows in Fig. 2(a).

2.3.3. Dataset 3 of real-time odor interferences under target gas

For the general cases of counteraction, dataset 3 without target gas may be not enough for validation of the proposed interference elimination model. Therefore, the condition when electronic nose was placed in some concentration of the target gas should also be studied. Similarly to dataset 2, a dataset 3 with length of 2480 points for each sensor was also obtained in continuous sampling way. This dataset is developed under reference formaldehyde gas and four odor interferences, respectively. In detail, we present the approximation positions for each object as follows. Formaldehyde exists in three approximated regions 102–250, 719–880 and 1380–1580; ethanol exists in region 260–410; toiletwater exists in region 881–1064; a hybrid interference of perfume and orange is located in region 1599–1899. The approximated target gas and interference regions have been illustrated by six Rectangular windows in Fig. 2(b).

Table 1
Concentrations of the six indoor air contaminants.

Formaldehyde data (CH_2O)

(15,60)	(15,80)	(20,40)	(20,60)	(20,80)	(25,40)	(25,60)	(25,80)	(30,40)	(30,60)	(30,80)	(35,60)
0.04	0.14	0.07	0.10	0.08	0.13	0.24	0.06	0.23	0.13	0.09	0.04
0.05	0.16	0.07	0.07	0.06	0.45	0.10	0.25	0.39	0.15	0.02	0.09
0.08	0.72	0.16	0.15	0.11	0.31	0.26	1.04	1.37	0.22	0.25	0.81
0.12	0.10	1.32	0.09	0.28	0.52	2.11	0.02	0.58	2.06	0.09	0.16
0.64	0.34	0.60	0.23	1.10	0.22	0.37	0.11	0.52	0.08	0.13	0.58
0.21	1.22	0.61	0.17	0.13	0.49	0.05	0.04	0.02	0.23	0.43	0.04
0.25	0.13	0.16	0.16	0.15	0.07	0.01	0.27	0.09	0.27	0.76	0.12
0.06	0.26	2.62	0.20	0.25	0.30	0.11	0.33	0.12	0.29	1.15	0.45
0.05	0.52	0.45	0.21	0.35	0.26	0.17	0.79	0.56	0.31	2.42	0.39
0.18	0.69	0.05	0.22	0.59	0.23	0.24	1.01	0.68	0.56	2.01	0.61
0.22	2.29	0.08	0.24	1.16	0.04	0.17	1.29	0.92	1.01	2.30	1.62
0.12	2.45	1.16	0.24	1.88	1.01	0.27	1.93	1.31	1.06		0.22
0.19	0.12	3.13	0.60	1.17	1.09	0.12	2.17	2.37	1.65		0.31
0.20	1.06	0.48	0.77	1.83	2.62	0.17	0.26	0.01	1.84		0.32
0.52	1.44	0.60	1.23		0.06	0.24	1.01	0.09	0.08		0.39
...	...	...	...		...	...	...	...	...		...

Benzene data (C_6H_6)

(15,60)	(15,80)	(20,40)	(20,60)	(20,80)	(25,40)	(25,60)	(25,80)	(30,40)	(30,60)	(30,80)	(35,60)
0.17	0.17	0.17	0.17	0.17	0.17	0.17	0.17	0.17	0.17	0.17	0.17
0.28	0.28	0.28	0.28	0.28	0.28	0.28	0.28	0.28	0.28	0.28	0.28
0.49	0.49	0.49	0.49	0.49	0.49	0.49	0.49	0.49	0.49	0.49	0.49
0.91	0.91	0.91	0.91	0.91	0.91	0.91	0.91	0.91	0.91	0.91	0.91
0.71	0.71	0.71	0.71	0.71	0.71	0.71	0.71	0.71	0.71	0.71	0.71
0.11	0.06	0.09	0.08	0.20	0.19	0.15	0.15	0.19	0.15	0.20	0.14
0.18	0.20	0.07	0.15	0.06	0.10	0.13	0.06	0.18	0.18	0.13	
0.25	0.21	0.25	0.21	0.14	0.21	0.14	0.14	0.08	0.10	0.24	
0.18	0.11	0.26	0.36	0.16	0.18	0.19	0.16	0.24	0.19	0.22	
0.24	0.30	0.18	0.42	0.21	0.33	0.20	0.16	0.25	0.30		
0.32	0.22	0.06	0.43	0.21	0.16	0.10	0.20	0.18	0.41		
0.11	0.26	0.11				0.17	0.21	0.24			

Toluene data (C_7H_8)

(15,60)	(15,80)	(20,40)	(20,60)	(20,80)	(25,40)	(25,60)	(25,80)	(30,40)	(30,60)	(30,80)	(35,60)
0.05	0.05	0.05	0.05	0.06	0.05	0.05	0.05	0.05	0.05	0.05	0.05
0.08	0.06	0.08	0.06	0.08	0.06	0.06	0.06	0.06	0.06	0.06	0.06
0.14	0.14	0.14	0.14	0.14	0.14	0.14	0.14	0.14	0.14	0.14	0.14
0.06	0.08	0.06	0.08	0.05	0.08	0.08	0.08	0.08	0.08	0.08	0.08

Carbon monoxide data (CO)

(15,60)	(15,80)	(20,40)	(20,60)	(20,80)	(25,40)	(25,60)	(25,80)	(30,40)	(30,60)	(30,80)	(35,60)
6	4	6	5	5	6	4	5	5	14	4	5
11	23	12	22	22	24	8	23	8	29	16	13
43	43	41	43	44	46	10	45	23	49	48	20
23	12	22	11	12	14	21	33	37	55	13	29
		13	9	20	10	12	48	6	25	16	20

Ammonia data (NH_3)

(15,60)	(15,80)	(20,40)	(20,60)	(20,80)	(25,40)	(25,60)	(25,80)	(30,40)	(30,60)	(30,80)	(35,60)
0.10	0.28	0.34	0.80	0.98	0.09	0.33	0.27	0.66	0.79	0.20	0.28
0.50		1.72	0.79	0.44	0.53	0.79	0.73	0.09	0.92	0.36	2.15
0.25		0.80			0.12	0.55			1.18		0.27

Nitrogen dioxide data (NO_2)

(15,60)	(15,80)	(20,40)	(20,60)	(20,80)	(25,40)	(25,60)	(25,80)	(30,40)	(30,60)	(30,80)	(35,60)
0.09		0.03	0.16	0.10	0.12	0.15	0.03		0.21		
0.20	-	0.92	0.84	0.54	0.31	0.22	0.05	-	0.61	-	-
1.62		0.77	0.28	0.18	0.20	0.70	0.87		1.36		
0.66						0.02	1.59				
							0.07				
							0.17				

2.4. Feature selection of unwanted odor interference

Feature selection for representing the texture of unwanted smell being counteracted is a critical step for subsequent pattern analysis. Due to that the first six analytes are target gases in our project, thus, only the steady state responses of an array were selected as the texture of each target gas for each sample. However, for counteraction of odor interference, only steady state response is not enough because of the possible erroneous decision in adsorption and desorption process. Therefore, four features including adsorption, transient response point reflecting the sensor dynamics of the increasing/decaying transient, steady state response and desorption points were selected to express the texture of odor interference. Specifically, the adsorption and desorption positions

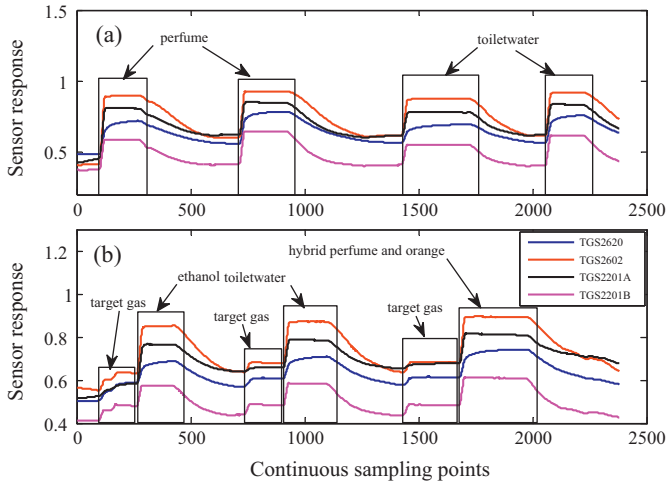

Fig. 2. Continuous real-time sampling curves of four sensors with odor interferences. (a) Denotes the observation signal for each sensor without target gases; (b) denotes the observation signal under some concentration of reference target gas. The Rectangular windows illustrate the actual regions of target gas and odor interferences in the two experiments.

are located at the 1/2 of the ascent stage and descent trajectory, respectively. Besides, the position of transient response is located at the maximum position of exponential moving average (*ema*) transform calculated by [28]

$$y[k] = (1-\alpha)\cdot y[k-1] + \alpha\cdot(r[k]-r[k-1]), \quad k = 1, \ldots, M \tag{3}$$

where r denotes the sensor observation vector, y denotes the *ema* vector, α is the smooth parameter within [0,1], and M denotes the length of the observation vector.

The reason for these selections is due to the considerations of the necessary sensitivity to unwanted odors, promptness and accuracy of the counteraction model. However, the adsorption and desorption positions (1/2) are not arbitrary, and they can be adjusted as requirement of model sensitivity. Fig. 3(a) illustrates the dynamic sensor response when exposed to perfume. The approximated positions for the selected features have been presented by vertical lines and arrows. Fig. 3(b) presents the *ema* curve with $\alpha = 0.05$. The position for transient response in Fig. 3(a) is the same position of the maximum *ema* in Fig. 3(b). The maximum *ema* of each sensor has been highlighted in an ellipse.

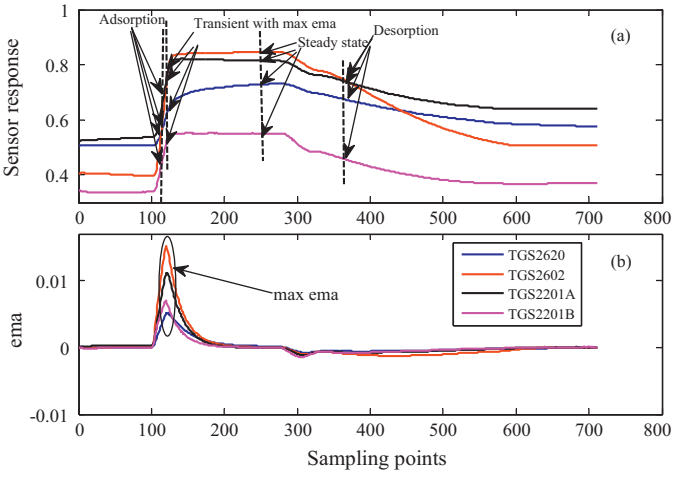

Fig. 3. Feature selection of odor interference; (a) describes the specific positions (adsorption, transient response, steady state response and desorption) of feature selection; (b) presents the *ema* curve with $\alpha = 0.05$ and determines the position of the maximum *ema* as the position of transient response.

2.5. Genetic crossover operator for solution of uneven features

In support vector multi-class problem and artificial neural network binary classification problem, uneven number of features for each class will lead to classification tendency. That is, that class with fewer samples can be easily discriminated as the class with more features, so that the accuracy and robustness of the classifier will degrade. Inspired by genetic algorithm (GA) [29], this paper introduces a new feature generation method based on genetic crossover operator to make the number of features for each class in the train set of LSSVM equilibrium. In genetic crossover operation, parts of genes in two pairs of chromosomes exchange in a certain way and two new individuals can be produced. The arithmetic crossover operator adopted in the present study is shown by

$$\begin{cases} p_1' = p_1 \cdot rand + p_2 \cdot (1 - rand) \\ p_2' = p_1 \cdot (1 - rand) + p_2 \cdot rand \end{cases} \tag{4}$$

where p_1 and p_2 denote the parent features, p_1' and p_2' represent the new child features and *rand* denotes a random value within [0,1].

For each generation, we randomly select two parent features and get two new children features, and repeat this step until the train features for each class are balanced. To check up the characteristic of distribution between the new children features and the parent features space, the Euclidean distance d_i between the i-th new child sample p_i' and the *center* of the parent features for each class was calculated by

$$d_i = \left\| p_i' - center \right\|_2 \tag{5}$$

The center of the parent features for each class can be calculated by

$$center = \frac{1}{m} \cdot \sum_{i=1}^{m} X_i \tag{6}$$

Through comparison with the tolerated *threshold* which was defined as the maximum Euclidean distance between each parent sample p_i and the center of parent features.

$$\text{Threshold} = \max_i \{ \left\| p_i - center \right\|_2 \}, \quad i = 1, \ldots, m \tag{7}$$

The trade-off of the new child sample p_i' for each class can be shown by

$$if \quad d_i \le threshold, \quad accept \quad p_i'; \quad else, \quad refuse \quad p_i' \tag{8}$$

2.6. Learner-1 under multi-class condition

SVM, as a novel machine learning method based statistical theory, was proposed in [30]. It has advantages of strong robustness, dimension insensitivities and structural risk minimum. Consider the high complexity of the optimization solution of SVM based on inequality constraint, the least square support vector machine (LSSVM) algorithm which transforms the inequality constraint into equality constraint by introducing a slack variable [31] is adopted for multi-class classification (learner-1) in this paper. ANN is developed for a binary classification problem (learner-2).

2.6.1. Multi-class LSSVM

Learner-1 is designed for counteraction under a multi-class condition [25]. That is, the unwanted odors were discriminated in a complex multi-class problem. Therefore, LSSVM was used for consideration of its strong classification ability. Multi-class problem has often been transformed into a binary classification problem. Two methods for commonly solving multi-class problems are "one-against-all (OAA)" and "one-against-one (OAO)" [32]. OAO strategy

has become a better recommendation choice when the number of classes $k \leq 10$ [33]. Therefore, OAO strategy was selected for $k = 7$ classes problem in this presented study. That is, $k(k-1)/2 = 21$ binary classifiers would be designed for final decision based on a simple voting scheme. The class with the most polls would be the final decision.

2.6.2. Nonlinear kernel function

In most cases, two classes cannot be linearly separated. In order to make the linear learning machine work well in non-linear cases, the original input space can be mapped through a nonlinear kernel function into some higher-dimensional feature space where the training set is linearly separable. In general, any positive semi-definite functions that satisfy the Mercer's condition can be kernel functions [34]. Some most widely used kernels contain linear kernel, polynomial kernel, Gaussian radial basis function (RBF), and sigmoid kernel. In this study, RBF kernel shown below has been used for high dimension transformation.

$$K(x_i, x) = \exp\left(-\frac{\left\|x - x_i\right\|^2}{\sigma^2}\right) \quad (9)$$

where σ_2 is kernel parameter. For each binary classifier, the non-linear decision function is shown as

$$f(x) = \text{sign}\left[\sum_{i=1}^{l} \alpha_i \cdot K(x_i, x) + b\right] \quad (10)$$

where α and b are trained by LSSVM.

2.6.3. Tuning of LSSVMs' parameters

LSSVMs have parameters to be tuned, which influence their performance. They are regularization parameters γ and the kernel parameters σ^2. As multi-class problem, each classifier has a pair of γ and σ^2, thus, 21 pairs of tuning parameters were obtained through simulated annealing (SA) optimization and a grid-search method based on a minimum leave-one-out (LOO) cross-validation error as cost function. SA is a heuristic optimization method based on the motivation from how crystalline structures are formed from annealing process and SA has a potential of finding an optimal solution when provided enough time for the annealing process [35]. In the LSSVM tuning procedure, SA was called as a global search at the first step and then grid-search was prepared for a local search in a limited region. In detail, the LS-SVM Toolbox and its principle including the specific functions call can be seen in [36].

2.7. Learner-2 under binary classification condition

For comparison with learner-1 under a multi-class condition, learner-2 is designed through a simple binary classification with only two classes (target gases class and odor interferences class). That is, we combine the six kinds of target gases together, and recognize them as the same class. For convenient analysis, labels "000" and "100" are assigned to target gases class and odor interferences class, respectively. For such binary classification, a two-hidden layered back-propagation neural network (BPNN) was trained and tested in dataset 1. In the present work, 10 neurons in each hidden layer were used. The training goal for BP convergence is set as 0.05. The structure of the ANN is $6 \times 10 \times 10 \times 3$. The active functions of the hidden layers ant output layer are selected as log-sigmoid and pure linear function. The log-sigmoid function can be shown by

$$f(x) = \frac{1}{1 + \exp(-x)} \quad (11)$$

The outputs need a further process of 0 and 1 through a simple comparison with the threshold 0.5. It can be seen that learner-2 is easier to understand and be implemented than learner-1. Learner-2 also implies that any observation signal which is not correlated with target gases would also be recognized as odor interference. Therefore, learner-2 is still reliable to the unwanted interferences not presented in this work.

2.8. Adaptive counteraction model of odor interference

2.8.1. Dynamical target signal matrix storage and updating

Before signal correction, a dynamical target signal matrix P with size of $m \times n$ would be first built, where m is the dimension of sensor array and n is the length of P. The matrix P is generated in real time E-nose application. The storage and updating process of P can be illustrated as follows

Step 1: Set a null matrix P with size of $m \times n$.

Step 2: A group of sensor signal column vector x in an E-nose is obtained.

Step 3: Analyze the x using the well-trained learner and a class label T of x is obtained from the learner.

Step 4: If $T = 0$ (target gas), x is stored into P, then go to step 5; else abandon x, return to *step 2*.

Step 5: If P is full ($x_1, x_2, \ldots, x_n$ have been fully stored), then the new x_{n+1} with $T = 0$ will hold the position of x_n, the x_n will hold the position of x_{n-1}, the x_{n-1} will hold the position of x_{n-2}, . . ., the x_2 will hold the position of x_1, and x_1 will be erased.

Step 6: Return to *step 2*, a dynamical target signal matrix P is then produced and updated on-line.

2.8.2. On-line signal correction

On the basis of the classification learner-1 and learner-2 presented in this study, the on-line correction model of odor interferences to MOS sensors can be illustrated as

$$y_i = \begin{cases} f(x_i), \text{ if } x_i \in \text{unwanted odor disturbances} \\ x_i, \text{ if } x_i \notin \text{unwanted odor disturbances} \end{cases}, \quad i = 1, 2, 3, 4 \quad (12)$$

where x_i denotes the real-time observation response of the i-th sensor (4 MOS sensors presented), y_i represents the response of the i-th sensor after counteraction of interference, and $f(\cdot)$ defines the counteraction function which can be presented as a linear model $f(x) = h \cdot x$ for simplification. The coefficient h ($0 < h \leq 1$) can be defined in terms of the current signal $x_{i,\text{curr}}$ (with interference) and the previous signal vector $P_{i,\text{pre}}$ of n sampling points with the nearest time interval (without interference) as follows

$$h_i = \min_n \frac{P_{i,\text{pre}}}{x_{i,\text{curr}}} \quad i = 1, 2, 3, 4 \quad (13)$$

Note that the length of the previous signal vector $P_{i,\text{pre}}$ is n and the sampling frequency is 1 Hz. The length of n is set to 50 in this paper, which can be adjusted as requirement of actual application. For clear understanding of the background counteraction model, the structure of the presented method has been illustrated in Fig. 4.

2.9. Software

All algorithms for interference counteraction in this paper were implemented in MATLAB 2009a, operating on a laboratory computer equipped with Inter Core (TM) i3 CPU 530, 2.93 GHz processors and 2 GB of RAM. The LSSVM classification was operated using LS-SVMlab Toolbox version 1.8 [36].

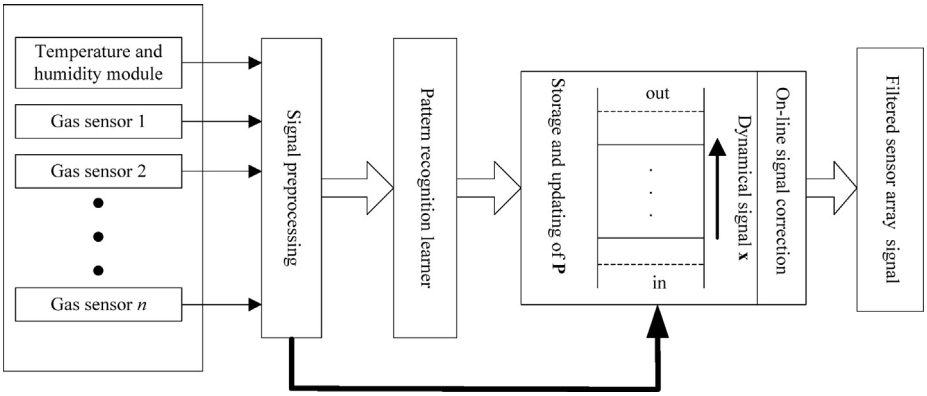

Fig. 4. Structure of the presented background interferences counteraction method.

Table 2
Recognition accuracy of learner-1 for interferences detection in E-nose.

Classes	ACA (%)		MCA (%)	
	Train data	Test data	Train data	Test data
Formaldehyde	97.16 ± 1.0575	96.35 ± 0.7274	98.40	96.83
Benzene	98.04 ± 0.8570	91.67 ± 1.3176	99.20	95.83
Toluene	99.68 ± 0.4665	100.0 ± 0.0000	100.0	100.0
Carbon-monoxide	99.36 ± 0.8237	94.50 ± 2.1794	100.0	100.0
Ammonia	98.84 ± 0.9625	97.25 ± 2.4875	100.0	100.0
Nitrogen-dioxide	99.24 ± 0.8570	76.92 ± 5.4393	100.0	84.62
Stimulus disturbance	97.72 ± 0.8495	97.30 ± 0.0000	98.40	97.30

3. Results and discussion

3.1. Recognition accuracy of learner-1 and learner-2 in E-nose

The LSSVM classifier (learner-1) was trained and tested on dataset 1 with genetic crossover operator for solution of uneven features including seven classes: formaldehyde, benzene, toluene, CO, NH_3, NO_2 and interferences. Totally, 875 (125 × 7) training samples were obtained. Thus, 21 binary classifiers have been designed based on LOO strategy. In LSSVM training process, we run the program 20 times on the train set and validate the classifier using the test set. Table 2 presents the average classification accuracy (ACA), standard deviation (±) and maximum classification accuracy (MCA) of the 20 runs including train accuracy and test accuracy. From the low standard deviation of the train data and test data, LSSVM classifier has a good stability. The designed classifier has a stable recognition of odor interferences with classification accuracy 97.3% for each run. For other target gases except NO_2, the classification accuracy can satisfy recognition in this work. The classification accuracy of NO_2 is lower than other gases because it is oxidizing and produces negative response to MOS sensor of this study which is different with other gases.

Consider that the learner-2 is only trained by BPNN using two classes (target gases class and odor interferences class), the number of original training samples of target gas class is 320, and thus 320 samples were also obtained for odor interferences through the new sample generator presented in this paper. Totally, 640 training samples were obtained for BPNN. Table 3 presents the average classification accuracy and maximum classification accuracy of 20 runs including train accuracy and test accuracy. From the results, we find that the accuracies for target gases class and interferences class in test data are 99.38% and 97.30%. The variances are also low and learner-2 is better than learner-1. From the results of the test samples in dataset 1, we cannot evaluate the stand or fall of learner-1 and learner-2. However, only through benchmark analysis (model learning and testing) may be not enough. Therefore, we present a real-world case study on the background elimination model based on learner-1 and learner-2, respectively.

3.2. Real-world case study of unwanted odor interferences counteraction

3.2.1. Case study under the environment without target gas

For validation of the effectiveness of the presented on-line counteraction model, dataset 2 with real-time collection has been analyzed. Considering the similar and repetitive counteraction work of all sensors, we just present the results of TGS2620 sensor as an example. The similar counteraction results of other three gas sensors (TGS2602, TGS2201A/B) based on learner-1 and learner-2 were given in supplementary data. The discrimination and counteraction tasks are first studied based on learner-1 (Fig. 5) and learner-2 (Fig. 6) on the dataset 4 without target gas. Fig. 5 illustrates the validation results based on learner-1 and the presented counteraction model. It can be seen that the four actual regions of interferences shown in Fig. 2(a) have been recognized in Fig. 5 (the Rectangular windows). However, the region

Table 3
Recognition accuracy of learner-2 for interferences detection in E-nose.

Classes	ACA (%)		MCA (%)	
	Train data	Test data	Train data	Test data
Target gases	98.84 ± 0.0028	98.64 ± 0.0066	99.38	99.38
Interferences	98.85 ± 0.0031	95.41 ± 0.0124	99.07	97.30

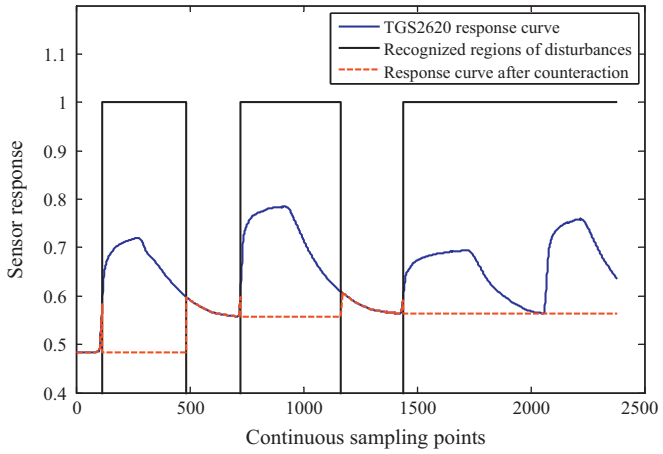

Fig. 5. Counteraction of odor interference based on learner-1 without target gas. The rectangular windows illustrate the recognized regions of odor interference; the dashed curve denotes the sensor response after counteraction.

between the third and fourth interference regions in Fig. 2(a) has also been recognized as interference region using learner-1 which is over positive. Fig. 6 describes the validation results based on learner-2 and the presented counteraction model. In Fig. 6, four regions have been recognized as interference regions which are consistent with the true regions shown in Fig. 2(a). From the interference recognitions, learner-2 is better than learner-1. However, from the interference counteraction curves (dashed lines) based on both models, the interference can be effectively eliminated.

3.2.2. Case study under the environment of target gas

The counteraction on the dataset 2 which has an abrupt change of sensor response may be a special case. Therefore, the counteraction should be studied in a general case that the interference appears under some concentration of target gas. The response curves of each sensor in dataset 3 have been presented in Fig. 2(b). Both target gas and interference appeared in dataset 3. The actual regions of target gas and interference were presented in Rectangular windows of Fig. 2(b). Fig. 7 illustrates the classification and counteraction of interferences based on learner-1 and the counteraction model. First, the regions in three Rectangular windows are represented as interferences discriminated by learner-1. However, the third region

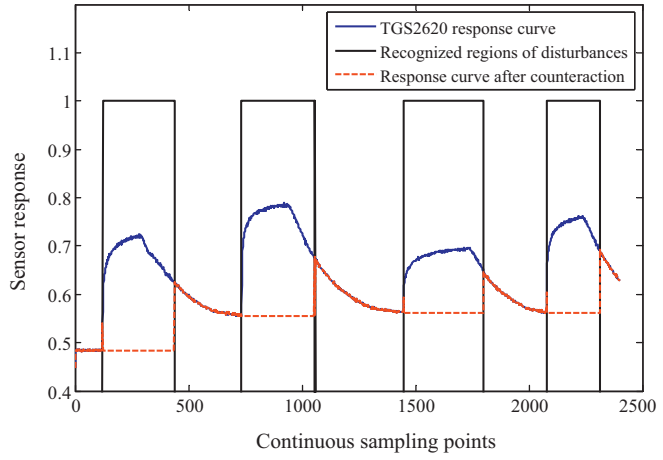

Fig. 6. Counteraction of odor interference based on learner-2 without target gas. The rectangular windows illustrate the recognized regions of odor interference; the dashed curve denotes the sensor response after counteraction.

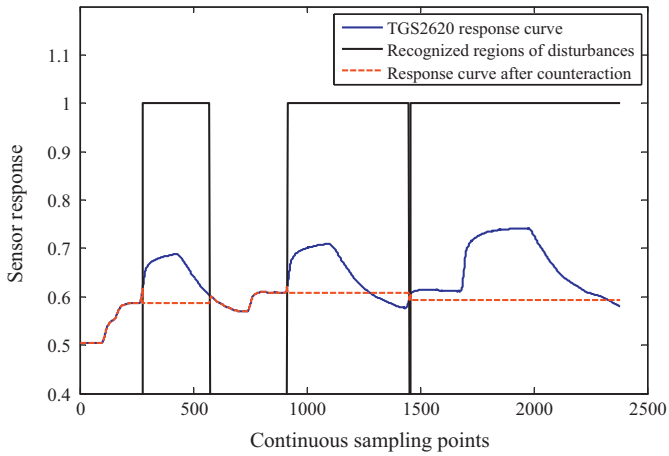

Fig. 7. Counteraction of odor interference based on learner-1 under some concentration of target gas.

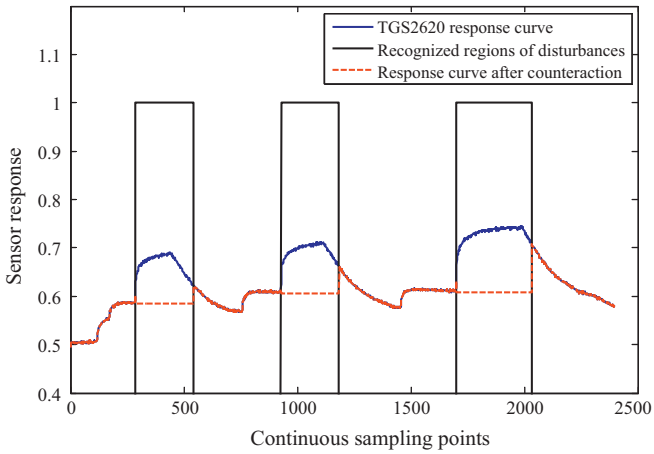

Fig. 8. Counteraction of odor interference based on learner-2 under some concentration of target gas.

of target gas was incorrectly recognized as interference. Besides, the second recognized interference region has been expanded compared with the true interference regions in Fig. 2(b). The discrimination regions in Fig. 7 also demonstrate that the learner-1 is over-positive. Similarly, Fig. 8 presents the analysis based on learner-2 and the counteraction model. Also, three regions in Rectangular windows are recognized as interference and keep consistent with the true regions shown in Fig. 2(b). The dashed lines in Figs. 7 and 8 denote the TGS2620 response curve after interference counteraction. From the comparisons of both Figs. 7 and 8, the learner-2 is better than learner-1 from the interference recognition regions. However, the counteraction results based on both learners can be accepted. From the response curve (dashed line) after counteraction, we can see that the signal with interference has been effectively reduced and counteracted.

4. Discussion

However, there is still a problem about the location of the interference boundaries. Seen from Figs. 6 and 8, for the correctly recognized regions of interference, the interference (desorption) in the descent process is recognized as target gas prematurely. Therefore, the response curves (dashed lines) after counteraction seem not to be very smooth. In terms of the solution of this problem, a possible way is to change the positions of adsorption and desorption in feature selection of interference in Fig. 3(a). For example,

the positions of adsorption and desorption points (1/2 is presented in this work) can be moved forward and backward, respectively, so that the recognition region for interference can be magnified. Consider the accuracy of recognition, we suggest the special positions for adsorption and desorption be determined at the middle position (1/2) in the adsorption and desorption process so that both accuracy and robustness of the E-nose instrument can be promised in practical environmental monitoring. From the construction of learner-1 and learner-2, learner-1 based on multi-class mechanism trained by LSSVM is more complex than learner-2 trained by BPNN based on binary classification rule. However, learner-2 performs better than learner-1 from the discrimination of target gas and interference. Since both of them can help the counteraction model realize the counteraction purpose, learner-2 based on binary rule is easier to be operated on-line by the FPGA processor in an E-nose.

Unwanted odor interference in an E-nose can not be tolerated because it can completely destroy the E-nose system for monitoring, and an E-nose will lose effect in target gases quantification monitoring when exposed to such interference. This presented research on interference counteraction of E-nose is a powerful compensation for our previous work in environmental gases quantification monitoring [21] and MOS sensors calibration transfer [17] in a large scale manufacture of E-nose instruments. In addition, the presented study is also novel and meaningful in electronic nose development. In LSSVM combined with genetic crossover operator, hybrid SA with grid-search in hyper-parameter tuning was used in this work, a possible improvement in the future is to apply genetic algorithm (GA) or particle swarm optimization (PSO) based evolutionary algorithm in tuning of LSSVM parameters γ, σ^2 [37,38] and training of LSSVM hyper-plane α, b [39].

5. Conclusions

In the present study, we successfully demonstrated the real-time application of the on-line unwanted odor interference counteraction model based on two artificial intelligence learners in electronic nose for the first time. With respect to the advantages of this machine learning technique in combination with MOS sensors of weak selectivity to target gases, we resolved the intrinsic high susceptibility to odor interferences problem of metal oxide semiconductor sensors and strengthen the prediction accuracy, robustness, and interference-counteraction characteristic of the environmental E-nose instruments. To meet the requirements of real-time environmental monitoring of pollutant gases, low complexity of model and feature selection of interference should be necessary. In this paper, learner-2 based on binary classification may be a better choice in background elimination of E-nose. Here, we also suggest focusing further efforts on the adsorption and desorption process for determining the appropriate boundaries in the future.

Acknowledgements

We would like to express our sincere appreciation to the anonymous reviewers for their insightful comments, which have greatly improved the quality of the paper. This work was supported by New Academic Researcher Award for Doctoral Candidates Granted by Ministry of Education and Hong Kong Scholar Program in China. This work was also supported by the Key Science and Technology Research Program (no. CSTC2010AB2002, CSTC2009BA2021).

Appendix A. Supplementary data

Supplementary data associated with this article can be found, in the online version, at http://dx.doi.org/10.1016/j.sna.2013.07.032.

References

[1] S.M. Scott, D. James, Z. Ali, Data analysis for electronic nose systems, Microchimica Acta 156 (2007) 183–207.
[2] S.M. Kanan, O.M. EI-Kadri, I.A. Abu-Yousef, M.C. Kanan, Semiconducting metal oxide based sensors for selective gas pollutant detection, Sensors 9 (2009) 8158–8196.
[3] C. Di Natale, R. Paolesse, A. Macagnano, A. Mantini, C. Goletti, A. D'Amico., Characterization and design of porphyrins-based broad selectivity chemical sensors for electronic nose applications, Sensors and Actuators B 52 (1998) 162–168.
[4] C. Di Natale, E. Martinelli, A.D. Amico, Counteraction of environmental disturbances of electronic nose data by independent component analysis, Sensors and Actuators B 82 (2002) 158–165.
[5] M. Holmberg, F.A.M. Davide, C. Di Natale, A. D'Amico, F. Winquist, I. Lundström, Drift counteraction in odour recognition applications: lifelong calibration method, Sensors and Actuators B 42 (1997) 185–194.
[6] E.J. Wolfrum, R.M. Meglen, D. Peterson, J. Sluiter, Calibration transfer among sensor arrays designed for monitoring volatile organic compounds in indoor air quality, IEEE Sensors Journal 6 (2006) 1638–1643.
[7] S.K. Jha, R.D.S. Yadava, Denoising by singular value decomposition and its application to electronic nose data processing, IEEE Sensors Journal 11 (2011) 35–44.
[8] F. Hossein-Babaei, V. Ghafarinia, Compensation for the drift-like terms caused by environmental fluctuations in the responses of chemoresistive gas sensors, Sensors and Actuators B 143 (2010) 641–648.
[9] J.H. Sohn, M. Atzeni, L. Zeller, G. Pioggia, Characterisation of humidity dependence of a metal oxide semiconductor sensor array using partial least squares, Sensors and Actuators B 131 (2008) 230–235.
[10] M. Holmberg, F. Winquist, I. Lundström, F. Davide, C. DiNatale, A. D'Amico, Drift counteraction for an electronic nose, Sensors and Actuators B 35/36 (1996) 528–535.
[11] M. Padilla, A. Perera, I. Montoliu, A. Chaudry, K. Persaud, S. Marco, Drift compensation of gas sensor array data by orthogonal signal correction, Chemometrics and Intelligent Laboratory Systems 100 (2010) 28–35.
[12] A. Ziyatdinov, S. Marco, A. Chaudry, K. Persaud, P. Caminal, A. Perera, Drift compensation of gas sensor array data by common principal component analysis, Sensors and Actuators B 146 (2010) 460–465.
[13] H. Ding, J.H. Liu, Z.R. Shen, Drift reduction of gas sensor by wavelet and principal component analysis, Sensors and Actuators B 96 (2003) 354–363.
[14] M. Paniagua, E. Llobet, J. Brezmes, X. Vilanova, X. Correig, E.L. Hines, On-line drift counteraction for metal oxide gas sensor arrays, Electronic Letters 39 (2003) 40–42.
[15] O. Tomic, H. Ulmer, J.E. Haugen, Standardization methods for handling instrument related signal shift in gas sensor array measurement data, Analytica Chimica Acta 472 (2002) 99–111.
[16] E.J. Wolfrum, R.M. Meglen, D. Peterson, J. Sluiter, Calibration transfer among sensor arrays designed for monitoring volatile organic compounds in indoor air quality, IEEE Sensor Journal 6 (2006) 1638–1643.
[17] L. Zhang, F.C. Tian, C. Kadri, B. Xiao, H. Li, L. Pan, H. Zhou, On-line sensor calibration transfer among electronic nose instruments for monitor volatile organic chemical in indoor air quality, Sensors and Actuators B 160 (2011) 899–909.
[18] A.K. Pavlou, N. Magan, J.M. Jones, J. Brown, P. Klatser, A.P.F. Turner, Detection of mycobacterium tuberculosis (TB) in vitro and situ using an electronic nose in combination with a neural network system, Biosensors and Bioelectronics 20 (2004) 538–544.
[19] B. Dębska, B. Guzowska-Świder, Application of artificial neural network in food classification, Analytica Chimica Acta 705 (2011) 283–291.
[20] B. Podola, M. Melkonian, Genetic programming as a tool for identification of analyte-specificity from complex response patterns using a non-specific whole-cell biosensor, Biosensors and Bioelectronics 33 (2012) 254–259.
[21] L. Zhang, F.C. Tian, C. Kadri, G. Pei, H. Li, L. Pan, Gases concentration estimation using heuristics and bio-inspired optimization models for experimental chemical electronic nose, Sensors and Actuators B 160 (2011) 760–770.
[22] C. Di Natale, A. Macagnano, E. Martinelli, R. Paolesse, G. D'Arcangelo, C. Roscioni, A.F. Agrò, A. D'Amico, Lung cancer identification by the analysis of breath by means of an array of non-selective gas sensors, Biosensors and Bioelectronics 18 (2003) 1209–1218.
[23] O.F. Canhoto, N. Magan, Potential for detection of microorganisms and heavy metals in potable water using electronic nose technology, Biosensors and Bioelectronics 18 (2003) 751–754.
[24] K. Brudzewski, S. Osowski, T. Markiewicz, Classification of milk by means of an electronic nose and SVM neural network, Sensors and Actuators B 98 (2004) 291–298.
[25] L. Zhang, F.C. Tian, H. Nie, L. Dang, G. Li, Q. Ye, C. Kadri, Classification of multiple indoor air contaminants by an electronic nose and a hybrid support vector machine, Sensors and Actuators B 174 (2012) 114–125.
[26] S.J. Dixon, R.G. Brereton, Comparison of performance of five common classifiers represented as boundary methods: Euclidean distance to centroids, linear discriminant analysis, quadratic discriminant analysis, learning vector quantization and support vector machines, as dependent on data structure, Chemometrics and Intelligent Laboratory Systems 95 (2009) 1–17.
[27] H.L. Chen, D.Y. Liu, B. Yang, J. Liu, G. Wang, A new hybrid method based on local fisher discriminant analysis and support vector machines for hepatitis disease diagnosis, Expert Systems with Applications 38 (2011) 11796–11803.

[28] M.K. Muezzinoglu, A. Vergara, R. Huerta, N. Rulkov, M.I. Rabinovich, A. Selverston, H.D. Abarbanel, Acceleration of chemo-sensory information processing using transient features, Sensors and Actuators B 137 (2) (2009) 507–512.
[29] D.E. Goldberg, Genetic algorithms in Search, Optimization, in: and Machine Learning, Addison Wesley, 1989.
[30] V. Vapnik, The Nature of Statistical Learning Theory, Springer, New York, 1995.
[31] J.A.K. Suykens, J. Vandewalle, Least square support vector machine classifiers, Neural Processing Letters 9 (3) (1999) 293–300.
[32] C.W. Hsu, C.J. Lin, A comparison of methods for multiclass support vector machines, IEEE Transactions on Neural Networks 13 (2002) 415–425.
[33] L.H. Chiang, M.E. Kotanchek, A.K. Kordon, Fault diagnosis based on Fisher discriminant analysis and support vector machines, Computers & Chemical Engineering 28 (2004) 1389–1401.
[34] B. Scholkopf, A.J. Smola, Learning with Kernels: Support Vector Machines, Regularization, Optimization, and Beyond, MIT Press, 2002.
[35] R.E. Burkard, F. Rendl, A thermodynamically motivated simulation procedure for combinatorial optimization problems, European Journal of Operational Research 17 (1984) 169–174.
[36] K. De Brabanter, P. Karsmakers, F. Ojeda, C. Alzate, J. De Brabanter, K. Pelckmans, B. De Moor, J. Vandewalle, J.A.K. Suykens, 2011, http://www.esat.kuleuven.be/sista/lssvmlab/.pdf
[37] X.C. Guo, J.H. Yang, C.G. Wu, C.Y. Wang, Y.C. Liang, A novel LS-SVMs hyper-parameter selection based on particle swarm optimization, Neurocomputing 71 (2008) 3211–3215.
[38] A.C. Lorena, A.C.P.L.F. de Carvalho, Evolutionary tuning of SVM parameters values in multiclass problems, Neurocomputing 71 (2008) 3326–3334.
[39] X. Tang, L. Zhuang, J. Cai, C. Li, Multi-fault classification based on support vector machine trained by chaos particle swarm optimization, Knowledge-Based Systems 23 (2010) 486–490.

Biographies

Lei Zhang received his Ph.D degree in June 2013 in Circuits and Systems from Chongqing University. He is currently a Hong Kong scholar in the Hong Kong Polytechnic University. He was honored by New Academic Researcher Award for Doctoral Candidates granted by Ministry of Education in China and Youth Innovation Award of Academician. His research interests include computational intelligence, pattern recognition, artificial olfactory system, and nonlinear signal processing in Electronic Nose.

Fengchun Tian received Ph.D. degree in 1997 in Electrical Engineering from Chongqing University. He is currently a professor with the College of Communication Engineering of Chongqing University. His research interests include Electronic nose technology, artificial olfactory systems, pattern recognition, chemical sensors, signal/image processing, wavelet, and computational intelligence. In 2006 and 2007, he was recognized as a part-time Professor of GUELPH University, Canada.

Lijun Dang received her Bachelor degree in School of Electronic and Information Engineering in 2011 from the Dalian University of Technology, China; from September 2011 to June 2014, she studied for a MS degree in circuits and system. Her research interests include circuits and system design in electronic nose technology.

Guorui Li received his Bachelor degree in College of Communication Engineering in 2010 from the Chongqing University, China; from September 2010 to June 2013, he studied for a MS degree in circuits and system. His research interests include signal processing in electronic nose technology.

Xiongwei Peng received his Bachelor degree in Communication Engineering in 2012 from the Chongqing University, China; he is presently with Chongqing University, pursuing his MS degree in signal and information processing. His research interests include pattern recognition and signal processing in electronic nose technology.

Xin Yin received his Bachelor degree in Communication Engineering in 2012 from the Chongqing University, China; he is presently with Chongqing University, pursuing his MS degree in signal and information processing. His research interests include circuit design in electronic nose technology.

Shouqiong Liu is now a senior engineer of Academy of Metrology and Quality Inspection, Chongqing. Her research interest was mainly analytical chemistry.